

Pulse area dependence of multiple quantum coherence signals in dilute thermal gases

Benedikt Ames,¹ Andreas Buchleitner,^{1,2} Edoardo G. Carnio,^{1,2} and Vyacheslav N. Shatokhin^{1,2, a)}

¹⁾Physikalisches Institut, Albert-Ludwigs-Universität Freiburg, Hermann-Herder-Str. 3, D-79104 Freiburg, Germany

²⁾EUCOR Centre for Quantum Science and Quantum Computing, Albert-Ludwigs-Universität Freiburg, Hermann-Herder-Str. 3, D-79104 Freiburg, Germany

(Dated: June 12, 2022)

In the general framework of open quantum systems, we assess the impact of the pulse area on single and double quantum coherence (1QC and 2QC) signals extracted from fluorescence emitted by dilute thermal gases. We show that 1QC and 2QC signals are periodic functions of the pulse area, with distinctive features which reflect the particles' interactions via photon exchange, the polarizations of the laser pulses, and the observation direction.

I. INTRODUCTION

If an ensemble of two-level atoms in their electronic ground states is driven by a resonant laser pulse, photoabsorption events will trigger *dispersive* interactions between transition dipoles of excited and unexcited particles^{1,2}, which are of paramount fundamental and practical importance in atomic, molecular, and chemical physics. Through the particles' polarizability, these interactions modify the system's refractive index responsible for wave dispersion³, hence their name. A common manifestation of dispersive interactions are collective shifts of the energy levels of a many-body system⁴. However, in a *dilute thermal* gas these shifts are negligibly small compared to the Doppler broadening introduced by thermal motion, rendering their sensing challenging. Nonetheless, ultrafast nonlinear optical spectroscopy⁵ provides tools to observe subtle features of the coupling between neutral particles, via measurements of so-called multiple quantum coherence (MQC) signals, which are an indication of collective excitations in interacting systems^{6,7} (see Fig. 1). In particular, it was shown that double-quantum coherence (2QC) signals appear only in the presence of level shifts induced by dipole-dipole interactions⁸.

One of the most powerful methods to detect MQC signals in dilute thermal atomic ensembles is provided by non-linear two-dimensional electronic spectroscopy (2DES)^{9,10}. Although 2DES has proved to be a sensitive technique to probe dipolar interactions, it relies on measurements of the nonlinear response functions induced by a series of non-collinear, time-delayed fields^{5,9}. The interaction of the latter with a sample results in the emission of photon echo- or free-induction decay-type signals in directions satisfying phase-matching conditions⁹, which are different for distinct MQC signals⁵. However, fulfilling these conditions becomes increasingly more difficult at lower densities and for MQC signals of higher order.

This complication, as well as some experimental artifacts associated with 2DES¹¹ can be overcome by fluorescence detection-based phase modulated spectroscopy¹². In this method, one sends a series of collinear, phase-tagged pulses

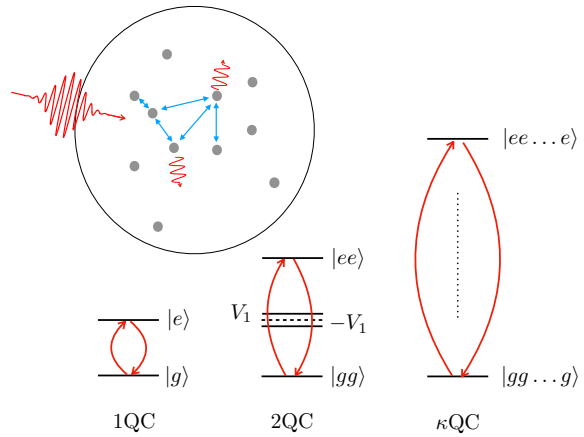


Figure 1. An external field incident on a cloud of neutral atoms induces dispersive interactions between transition dipoles. So-called single quantum coherence (1QC) signals emitted by the atoms are probes of single-particle dipole moments (coherences between the ground and excited states $|g\rangle$ and $|e\rangle$, respectively, of the individual atoms), while double quantum coherence (2QC) signals (in general, κ QC signals) are probes of a collective dipole moment of two (in general, κ) particles (coherence between the collective ground and excited state of a system of $2, \dots, \kappa$ particles). κ QC ($\kappa > 1$) signals are sensitive to shifts in the energy levels ($V_1, -V_1$ in the figure) induced by the dipole-dipole interactions (indicated by blue arrows), and therefore provide important information about collective excitations and interactions in many-body systems.

separated by one^{13,14} or several^{12,15} time delays onto a sample, and collects the fluorescence signal emitted by excited atoms in the transverse direction. The detected signal encodes, in particular, different orders of MQC signals, which can be individually extracted via demodulation. With these techniques, successful measurements of κ QC signals in dilute thermal gases with $\kappa \leq 7$ were reported^{14–16}. Since MQC spectra in fluorescence-based measurements originate from excited state populations, rather than coherences of atoms, early results¹⁴ initiated a debate^{16–19} whether the detected signals actually do certify dipole-dipole interactions in dilute, inhomogeneously broadened atomic clouds.

Recently, we put forward a microscopic theory of MQC

^{a)}Electronic mail: vyacheslav.shatokhin@physik.uni-freiburg.de

signals in dilute thermal gases which allowed us to resolve this controversy²⁰. Our theory includes several ingredients that have not been accounted for previously, such as the full form of the light-induced dipole-dipole interactions featuring both, *near-field* (or *electrostatic*) and *far-field* (or *radiative*) contributions, the vector character of the atomic dipole transitions as well as of the radiation field of the incoming laser pulses, and the unavoidable configuration (or disorder) average in a system of randomly located and mobile scatterers. We showed that interactions are actually crucial for the observations of κ QC signals, but they are mediated not by the hitherto considered^{16,18} electrostatic form of the dipole-dipole interactions, scaling as $\sim r^{-3}$, with r the interatomic distance, but by the light-induced far-field dipolar interactions scaling as $\sim r^{-1}$. As distinct from the electrostatic interaction, which only generates collective level shifts, the far-field interaction mediates both, collective level shifts and collective decay processes, both of which are crucial for the emergence of κ QC signals. In the chemical physics literature, such far-field interactions via real photon exchange are known as cascading^{21,22} or wave mixing processes²³. Therefore, our results may also be beneficial for the understanding of multi-quantum coherence signals in multilevel isolated chromophores²⁴, where cascading events are a source of noise.

A distinctive feature of our approach is its non-perturbative character with respect to the strength of the driving field. Previously²⁰ we calculated MQC signals with parameters as in the experiment in Ref. 16. In particular, the relatively weak laser pulses allowed us to treat the atom-laser interaction perturbatively, and to obtain good qualitative agreement with the experiment. Yet, it is well known that stronger pulses induce *nonlinear atomic responses of higher order*⁵, which may lead to novel features of MQC signals. In the present work, we identify these features and ponder how they can be used to understand better the interplay between laser-atom and dipole-dipole interactions. In addition, we treat the atomic motion more accurately than in our earlier work²⁰, and thereby obtain not only qualitative, but also quantitative agreement of our simulations with the experimentally observed, Doppler broadened line shapes of the complex 1QC and 2QC spectra.

The paper is structured as follows: In the next section, we equip the reader with the relevant background information. Thereafter, in Sec. III, we obtain inhomogeneously broadened 1QC and 2QC spectra in different observation directions and for different polarizations of the laser fields. Finally, we analyze the behavior of the spectral peaks as functions of the pulse area. Section IV concludes this work.

II. BACKGROUND

We set out with a brief description of the experimental setup for the observation of MQC signals. In Sec. II C, we lay out our main theoretical tool, a master equation governing the dynamics of a multi-atom, dipole-dipole interacting system excited by laser fields. Section II D outlines the main steps towards an analytical solution of the master equation. From this solution, the average fluorescence intensity is obtained

upon configuration average, which is explained in Sec. II E. Finally, in Sec. II F we show how 1QC and 2QC spectra follow from the fluorescence signal upon demodulation.

A. Fluorescence detection-based phase-modulated spectroscopy

In this spectroscopic approach, atoms are excited periodically by pairs of collinear, time delayed, ultrashort Gaussian pulses. For each cycle, the field in the frame rotating at the laser frequency ω_L has the time-dependent amplitude

$$\mathbf{E}_L(\mathbf{r}, t) = \sum_{j=1}^2 \boldsymbol{\varepsilon}_L^{(j)} \mathcal{E}_L(t - t_j) e^{i(\mathbf{k}_L \cdot \mathbf{r} + \omega_L t_j + w_j \tau_m)}, \quad (1)$$

where $\mathcal{E}_L(t') = \mathcal{E}_0 \exp(-t'^2/2\sigma^2)$ is the envelope, assumed to be the same for both pulses, with amplitude \mathcal{E}_0 and duration σ , and $\boldsymbol{\varepsilon}_L^{(j)}$ is the polarization of pulse j (in the following we will consider the cases $\boldsymbol{\varepsilon}_L^{(1)} = \boldsymbol{\varepsilon}_L^{(2)} = \hat{\mathbf{x}}$ and $\boldsymbol{\varepsilon}_L^{(1)} = \hat{\mathbf{x}}$, and $\boldsymbol{\varepsilon}_L^{(2)} = \hat{\mathbf{y}}$). Furthermore, $\phi_j = w_j \tau_m$ are phase tags imprinted on the pulses by transmitting them through two acousto-optic modulators oscillating at slightly different frequencies w_j ; these phase tags are proportional to $\tau_m = m T_{\text{cyc}}$, where T_{cyc} is the duration of one cycle, which is much longer than the natural lifetime of the atoms, and m counts the number of cycles in the experimental pulse train. After the interaction of the atoms with the second pulse at t_2 , the fluorescence intensity along a direction $\hat{\mathbf{k}} \perp \mathbf{k}_L$ is integrated by a photodetector until the cycle ends. Using a long pulse train with $m \gg 1$ cycles allows to sweep a broad range of phase tags ϕ_j and interpulse delays $\tau = t_2 - t_1$, which is a prerequisite for signal demodulation.

The signal to be demodulated is the transient intensity $I_{\hat{\mathbf{k}}}(\tau, t_{\text{fl}}, \phi_1, \phi_2)$ integrated over the fluorescence time t_{fl} ²⁵ which is approximated by the integral:

$$\bar{I}_{\hat{\mathbf{k}}}(\tau, \phi_1, \phi_2) = \int_0^\infty dt_{\text{fl}} I_{\hat{\mathbf{k}}}(\tau, t_{\text{fl}}, \phi_1, \phi_2). \quad (2)$$

This quantity remains congested with different harmonics of the modulation frequency, reflecting the interaction processes of atoms with the laser pulses as well as with one another. To select a specific modulation frequency component of the intensity, the recorded photocurrent $\bar{I}_{\hat{\mathbf{k}}}(\tau, \phi_1, \phi_2)$ is demodulated by multiplication with a reference signal $e^{-i\kappa w_{21} \tau_m}$ ($w_{21} = w_2 - w_1$ the modulation frequency, and κ the demodulation order – not by accident the same label as the order of the MQC signal above)^{14,26}. The current at the thus identified modulation frequency is experimentally extracted by a lock-in narrowband filter, tantamount of integrating the spectral intensity, within a Lorentzian frequency window of width $\sim \mathcal{F}$ centred around κw_{21} , over the pulse train's duration τ_m . Letting the filter width $\mathcal{F} \rightarrow 0$, the demodulated κ QC frequency spectrum is thus formally given by^{18,26}

$$S_{\hat{\mathbf{k}}}(\omega, \kappa) = \lim_{\mathcal{F} \rightarrow 0} \mathcal{F} \int_0^\infty d\tau_m e^{-(\mathcal{F} + i\kappa w_{21})\tau_m} \times \frac{1}{\sqrt{2\pi}} \int_0^\infty d\tau e^{-i\omega\tau} \bar{I}_{\hat{\mathbf{k}}}(\tau, \phi_1, \phi_2). \quad (3)$$

B. Physical system

We deal with a dilute thermal gas of alkali atoms at density $n \sim 10^7 - 10^{11} \text{ cm}^{-3}$ and temperature $\approx 320 \text{ K}$ ^{14,16}. Because of the thermal motion, a random spatial distribution of atoms in such a cloud is time-dependent; the coordinate of atom α is given by $\mathbf{r}_\alpha(t) = \mathbf{r}_{\alpha 0} + \mathbf{v}_\alpha t$, where $\mathbf{r}_{\alpha 0}$ and \mathbf{v}_α are, respectively, its initial coordinate and its velocity. We assume a homogeneous distribution of the initial coordinates $\mathbf{r}_{\alpha 0}$, while the Cartesian components of the velocities \mathbf{v}_α , drawn from the Maxwell-Boltzmann distribution for the given temperature, are typically $\sim 10^2 \text{ m/s}$. The atomic momentum at such velocities is several orders of magnitude larger than the photon momentum, which allows us to neglect the photon recoil effect and treat the atomic motion classically, i.e., ignore the coupling between the atomic external and internal degrees of freedom. Furthermore, because of the low atomic density n satisfying the inequality $n(\lambda/2\pi)^3 \ll 1$ (λ is the resonant optical wave length), the atoms are typically in each other's far-field, such that inter-atomic collisions can be neglected. We treat the atoms as an open quantum system embedded into a common quantized electromagnetic vacuum field. The interaction of the atoms with the latter gives rise to effective dipole-dipole interactions²⁷, upon tracing over the bath's degrees of freedom, and the atomic internal dynamics are then described by a master equation (see Sec. II C). Throughout this work, we unfold our formalism for a general system of N atoms, but carry out all calculations for $N = 2$. A system of two atoms suffices to evaluate 1QC and 2QC signals on which we focus in our present contribution; in any case, our model²⁰ includes all the essential ingredients of the physics characterizing a laser-driven, dilute thermal atomic ensemble.

The κ QC spectra are calculated, via (2) and (3), from the transient fluorescent intensity $I_{\hat{\mathbf{k}}}(\tau, t_{\text{fl}}, \phi_1, \phi_2)$, the quantum-mechanical expectation value of the intensity operator, averaged over atomic configurations. By definition²⁸, the time-dependent intensity is given by

$$I_{\hat{\mathbf{k}}}(t) = \left\langle \left\langle \mathbf{E}_{\hat{\mathbf{k}}}^{(-)}(t) \cdot \mathbf{E}_{\hat{\mathbf{k}}}^{(+)}(t) \right\rangle \right\rangle_{\text{conf}} \quad (4)$$

where $\langle \dots \rangle = \text{Tr}\{\dots \rho(0)\}$. The initial density operator $\rho(0)$ of the atoms-field system factorizes into the ground state of the atoms and the vacuum state of the field. The positive/negative frequency part $\mathbf{E}_{\hat{\mathbf{k}}}^{(+-)}(t)$ of the operator for the electric far-field can be expressed through the dipole operator of the source atoms α ²⁷,

$$\mathbf{E}_{\hat{\mathbf{k}}}^{(+)}(t) = f \sum_{\alpha=1}^N \left\{ \mathbf{D}_\alpha(t) - \hat{\mathbf{k}} [\hat{\mathbf{k}} \cdot \mathbf{D}_\alpha(t)] \right\} e^{-i\hat{\mathbf{k}} \cdot \mathbf{r}_\alpha(t)}, \quad (5)$$

where $f = \omega_0^2 d / (4\pi\epsilon_0 c^2 R_d)$, with ω_0 the unperturbed atomic transition frequency (and k_0 the associated wave number), d the transition dipole matrix element, c the speed of light, and R_d the distance from the center of mass of the atomic cloud to the detector. Moreover, \mathbf{k} is the wave vector of the scattered light, and $\mathbf{D}_\alpha^\dagger$, (\mathbf{D}_α) are atomic raising (lowering) operators which we choose to correspond to a $J_g = 0 \leftrightarrow J_e = 1$ transition in the concrete calculations presented in Sec. III. Note,

however, that all our subsequent expressions including dipolar operators are valid for transitions incorporating *arbitrary* degeneracies of the ground and excited state sublevels.

In writing (5), we assumed that $R_d \gg r_{\alpha\beta}(t) = |\mathbf{r}_\alpha(t) - \mathbf{r}_\beta(t)|$ for any α, β . Finally, $\langle \dots \rangle_{\text{conf}}$ in (4) stands for the configuration average. It results from the random initial positions of the many pairs of atoms in the cloud, and their thermal motion during the fluorescence detection time t_{fl} . We will treat the thermal velocities in an effective manner, such that our results ultimately involve integrations over the Maxwell-Boltzmann distributions of the Doppler shifts of moving atoms, as well as over the length and orientation of the vectors $\mathbf{r}_{\alpha\beta}$ connecting pairs of atoms. We denote the mean interatomic distance by \bar{r} , and assume an isotropic distribution of the atoms.

C. Master equation

With the aid of (5) the fluorescence intensity (4) reads

$$I_{\hat{\mathbf{k}}}(t) = \left\langle f^2 \sum_{\alpha, \beta=1}^N \langle \mathbf{D}_\alpha^\dagger(t) \cdot (\mathbb{1} - \hat{\mathbf{k}}\hat{\mathbf{k}}) \cdot \mathbf{D}_\beta(t) \rangle e^{i\hat{\mathbf{k}} \cdot \mathbf{r}_{\alpha\beta}(t)} \right\rangle_{\text{conf}}, \quad (6)$$

where $\mathbb{1}$ is a 3×3 unit matrix and $\hat{\mathbf{k}}\hat{\mathbf{k}}$ is a 3×3 dyadic. If the relative phase shift $k_0 v_\alpha r_{\alpha\beta}/c$ acquired by moving atoms within the photon propagation time (given by $r_{\alpha\beta}/c$) is small, i.e., $k_0 v_\alpha r_{\alpha\beta}/c \ll 1$ ²⁹, the time-dependent atomic dipole correlators entering Eq. (6) can be assessed via a Lehmburg-type master equation for arbitrary N -atom operators³⁰ (or, equivalently, for the N -atom density operator²⁷), under the standard Born and Markov approximation³¹. This condition is well fulfilled in a thermal dilute gas with $r_{\alpha\beta} \approx \bar{r} \sim 10 \mu\text{m}$ ³² and $k_0 v_\alpha \sim 600 \text{ MHz}$, where $k_0 v_\alpha r_{\alpha\beta}/c \sim 2 \times 10^{-5}$. We then obtain the same form of the dipole-dipole interaction as for immobile atoms, where the usually fixed interatomic distance $r_{\alpha\beta}$ acquires a time dependence²⁹.

For the quantum mechanical expectation value of an N -atom operator $Q = \otimes_{\alpha=1}^N Q_\alpha$, the master equation reads^{30,33} (written in the interaction picture with respect to the free-atoms Hamiltonian $\hbar\omega_0 \sum_{\alpha=1}^N \mathbf{D}_\alpha^\dagger \cdot \mathbf{D}_\alpha$):

$$\langle \dot{Q} \rangle = \left\langle (\mathcal{L}_L + \mathcal{L}_\gamma + \mathcal{L}_{\text{int}}) Q \right\rangle, \quad (7)$$

where $\mathcal{L}_L = \sum_{\alpha=1}^N \mathcal{L}_L^\alpha$, with \mathcal{L}_L^α the laser-atom interaction Liouvillian, $\mathcal{L}_\gamma = \sum_{\alpha=1}^N \mathcal{L}_\gamma^\alpha$, with $\mathcal{L}_\gamma^\alpha$ the relaxation Liouvillian describing the exponential decay of atomic excited state populations and of coherences, and $\mathcal{L}_{\text{int}} = \sum_{\alpha \neq \beta=1}^N \mathcal{L}_{\alpha\beta}$, with $\mathcal{L}_{\alpha\beta}$ the dipolar atom-atom interaction Liouvillian. The Liouvillians are given by³³⁻³⁵

$$\begin{aligned} \mathcal{L}_L^\alpha Q_\alpha &= -\frac{id}{\hbar} [\mathbf{D}_\alpha^\dagger \cdot \mathbf{E}_L(\mathbf{r}_{\alpha 0}, t) e^{-i\delta_\alpha t} \\ &\quad + \mathbf{D}_\alpha \cdot \mathbf{E}_L^*(\mathbf{r}_{\alpha 0}, t) e^{i\delta_\alpha t}, Q_\alpha], \end{aligned} \quad (8)$$

$$\mathcal{L}_\gamma^\alpha Q_\alpha = \frac{\gamma}{2} \left(\mathbf{D}_\alpha^\dagger \cdot [\mathcal{Q}_\alpha, \mathbf{D}_\alpha] + [\mathbf{D}_\alpha^\dagger, \mathcal{Q}_\alpha] \cdot \mathbf{D}_\alpha \right),$$

with

$$\delta_\alpha = \omega_L - \omega_0 - \mathbf{k}_L \cdot \mathbf{v}_\alpha \quad (9)$$

the laser-atom detuning modified by the Doppler effect, γ the single-atom spontaneous decay rate, and

$$\begin{aligned} \mathcal{L}_{\alpha\beta} Q_{\alpha\beta} &= \mathbf{D}_\alpha^\dagger \cdot \vec{\mathbf{T}}(k_0 r_{\alpha\beta}(t), \hat{\mathbf{n}}) \cdot [Q_{\alpha\beta}, \mathbf{D}_\beta] \\ &+ [\mathbf{D}_\beta^\dagger, Q_{\alpha\beta}] \cdot \vec{\mathbf{T}}^*(k_0 r_{\alpha\beta}(t), \hat{\mathbf{n}}) \cdot \mathbf{D}_\alpha, \end{aligned} \quad (10)$$

with the light-induced dipole-dipole interaction tensor $\vec{\mathbf{T}}(k_0 r_{\alpha\beta}(t), \hat{\mathbf{n}})$ for $\hat{\mathbf{n}} = \mathbf{r}_{\alpha\beta}/r_{\alpha\beta}$. Upon substitution $\xi(t) = k_0 r_{\alpha\beta}(t)$, the tensor $\vec{\mathbf{T}}(\xi(t), \hat{\mathbf{n}})$ reads

$$\begin{aligned} \vec{\mathbf{T}}(\xi(t), \hat{\mathbf{n}}) &= \frac{3\gamma}{4} e^{-i\xi(t)} \left[\frac{i}{\xi(t)} (\mathbb{1} - \hat{\mathbf{n}}\hat{\mathbf{n}}) \right. \\ &\left. + \left(\frac{1}{\xi(t)^2} - \frac{i}{\xi(t)^3} \right) (\mathbb{1} - 3\hat{\mathbf{n}}\hat{\mathbf{n}}) \right]. \end{aligned} \quad (11)$$

The real and imaginary parts of the tensor $\vec{\mathbf{T}} = \vec{\Gamma} + i\vec{\Omega}$ describe collective decay rates and collective level shifts²⁷. In the far-field limit, $\xi \gg 1$, which we here consider, Eq. (11) reduces to $\vec{\mathbf{T}}(\xi, \hat{\mathbf{n}}) \approx (3\gamma/4)g(\xi)[\mathbb{1} - \hat{\mathbf{n}}\hat{\mathbf{n}}]$, with coupling parameter $g(\xi) = ie^{-i\xi}/\xi$, $|g(\xi)| \ll 1$. In this regime, the collective decay rates and level shifts are, respectively,

$$\vec{\Gamma}(\xi, \hat{\mathbf{n}}) = \frac{3\gamma}{4} \frac{\sin \xi}{\xi} (\mathbb{1} - \hat{\mathbf{n}}\hat{\mathbf{n}}), \quad \vec{\Omega}(\xi, \hat{\mathbf{n}}) = \frac{3\gamma}{4} \frac{\cos \xi}{\xi} (\mathbb{1} - \hat{\mathbf{n}}\hat{\mathbf{n}}), \quad (12)$$

and describe dipolar interactions via the exchange of transverse photons³⁶.

D. Analytical solution of the master equation

1. Separation of timescales

The possibility of solving Eq. (7) analytically is based on the existence of several timescales characterising the system dynamics. The shortest timescale is set by the duration $\sigma \sim 50$ fs of the laser pulses. The typical interpulse delay $\tau \sim 10$ ps determines the second timescale. After the second pulse at time t_2 , atomic fluorescence is monitored for times t_{fl} , with $0 \leq t_{\text{fl}} \leq T_{\text{cyc}} - t_2 \sim 100\gamma^{-1}$, until all atoms with the natural lifetime $\sim \gamma^{-1} \approx 30$ ns³⁷ undergo a transition to their ground states, emitting photons. Thus, fluorescence detection establishes the long timescale, which typically lasts for about five orders of magnitude longer than the interpulse delay — for a few microseconds. Furthermore, on that long timescale, the typical thermal coherence time τ_{th} ³⁸ of the order of 10 ns³⁹ defines the regime of the atomic dynamics beyond which the Doppler effect is not negligible. In summary, the typical timescales satisfy the inequalities

$$\sigma \ll \tau \ll \tau_{\text{th}} \lesssim \underbrace{\gamma^{-1}}_{t_{\text{fl}}} \ll T_{\text{cyc}}. \quad (13)$$

The existence of several timescales that differ by orders of magnitude allows us to find approximate piecewise solutions of a simplified version of (7), which, on a given timescale, retains

only the relevant terms. Thus, during the shortest timescale we keep only the Liouvillian \mathcal{L}_L in (7). In contrast, between the pulses and after the second pulse, that is, during the intervals τ and t_{fl} , we retain $\mathcal{L}_Y + \mathcal{L}_{\text{int}}$ and ignore \mathcal{L}_L . We note that even though $\mathcal{L}_Y + \mathcal{L}_{\text{int}}$ is almost negligible during τ , these terms introduce some dephasing, without which MQC spectra for immobile atoms would represent delta peaks. Finally, using the weakness of the dipolar coupling, $|g(\xi)|\gamma \ll \gamma$, we solve (7) perturbatively with respect to \mathcal{L}_{int} .

For each subdomain of those piecewise solutions, we treat the atomic motion according to how long the respective intervals are compared to the thermal coherence time τ_{th} . Since $\tau_{\text{th}} \gg \sigma$, the atoms can be considered at fixed positions during the atom-laser interaction. For times exceeding τ_{th} , we instead perform a configuration average to account for the randomised atomic positions within the cloud (see Sec. II E).

2. Piecewise solutions

We now present operator solutions pertinent to the different timescales, σ , τ , and t_{fl} in (13), for some random atomic configuration. The evaluation of quantum-mechanical expectation values, and of the average over atomic positions and velocities of atoms, will follow in Sec. II E.

a. Interaction with laser pulses. During the shortest timescale σ , it is sufficient to solve the single-atom equation

$$\dot{Q}_\alpha = \mathcal{L}_L^\alpha Q_\alpha, \quad (14)$$

with \mathcal{L}_L^α given by (8). The action of the Liouvillian \mathcal{L}_L acting on an N -atom operator Q is then given by the tensor product of single-atom evolution operators.

Since the fast timescale associated with the laser pulses is much shorter than all other timescales, we replace the Gaussian laser pulses with delta pulses having the same pulse area. Then the action of pulse j on an atomic operator Q_α is reduced to an instantaneous unitary transformation (kick) R_j^α :

$$Q_\alpha(t_j^+) = R_j^\alpha Q_\alpha(t_j^-) = e^{-i\vartheta \mathcal{M}_j/2} Q_\alpha(t_j^-) e^{i\vartheta \mathcal{M}_j/2}, \quad (15)$$

where $Q_\alpha(t_j^-)$ ($Q_\alpha(t_j^+)$) is an atomic operator before (after) the kick,

$$\vartheta = \frac{2d}{\hbar} \int_{-\infty}^{\infty} dt' \mathcal{E}_L(t' - t_j), \quad (16)$$

is the pulse area, and \mathcal{M}_j is an atomic operator,

$$\mathcal{M}_j = S^\dagger e^{i\varphi_j} + S e^{-i\varphi_j}, \quad (17)$$

with $S^\dagger = \mathbf{D}_\alpha^\dagger \cdot \mathbf{e}_L$, $S = \mathbf{D}_\alpha \cdot \mathbf{e}_L^*$ the components of atomic raising and lowering operators along the laser polarization, and the phase

$$\varphi_j = \mathbf{k}_L \cdot \mathbf{r}_{\alpha 0} + \omega_0 t_j + w_j \tau_m + \Delta_\alpha t_j, \quad (18)$$

where $\Delta_\alpha \equiv \mathbf{k}_L \cdot \mathbf{v}_\alpha = k_L v_z^{(\alpha)}$ is the Doppler shift of atom α .

The transformation (15) is manifestly non-perturbative with respect to the pulse area (laser field strength). Using the algebraic properties of the operator \mathcal{M}_j , we obtain the following expansion of the superoperator R_j^α ⁴⁰:

$$R_j^\alpha = \sum_{l=-2}^2 e^{il\varphi_j} R_j^{[l]}. \quad (19)$$

with the φ_j -independent superoperators $R_j^{[l]}$ encoding the structure of the atomic dipole transition, the laser polarization, and the pulse area⁴⁰.

Let us recall that each laser-atom interaction cycle begins with the atoms prepared in their ground state $|g\rangle$. In this case, the expansion of R_1^α in (19) takes a simpler form, which we label $R_{1,g}^\alpha$, and only describes the action of the *first* pulse on a *ground-state* atom⁴⁰:

$$R_{1,g}^\alpha = \sum_{l=-1}^1 e^{il\varphi_1} R_{1,g}^{[l]}. \quad (20)$$

Since $l = -1, 0, 1$ in the above sum, the important consequence of (20) is that independent atoms cannot give rise to 2QC signals (see Sec. II F), which require terms $l = \pm 2$ in the sum.

b. Radiative decay and dipolar interactions. As discussed above in Sec. II D 1, during the inter-pulse and fluorescence harvesting intervals, respectively τ and $T_{\text{cyc}} - t_2$, we solve the master equation

$$\dot{Q} = (\mathcal{L}_\gamma + \mathcal{L}_{\text{int}})Q \quad (21)$$

perturbatively with respect to \mathcal{L}_{int} . Such solution can be most compactly represented with the aid of a Laplace transformations in the complex variable z , as

$$\tilde{Q}(z) = \sum_{n=0}^{\infty} \mathcal{G}_\gamma(z) \left[\mathcal{L}_{\text{int}} \mathcal{G}_\gamma(z) \right]^n Q(t_0), \quad (22)$$

where

$$\mathcal{G}_\gamma(z) = \int_0^\infty dt e^{-zt} e^{\mathcal{L}_\gamma t} = \frac{1}{z - \mathcal{L}_\gamma} \quad (23)$$

is the resolvent superoperator, $\tilde{x}(z) = \int_0^\infty dt' \exp(-zt')x(t')$, and $Q(t_0)$ corresponds to the N -atom operator at the beginning of the interval under consideration, i.e. $t_0 = t_1$ for the evolution during the interpulse delay, and $t_0 = t_2$ when collecting the fluorescence after the second pulse.

In the following, we examine 1QC and 2QC signals for $N = 2$ atoms that either are not interacting at all or exchange a single photon. These stem from single or double scattering contributions to the fluorescence signal. Formally, such contributions are described by the terms $n = 0, 2$ in the series expansion (22). By restricting ourselves to two atoms and double scattering, we exclude long scattering paths, which is justified in an optically thin medium^{33,41} as provided by a dilute thermal gas. Furthermore, in such medium we can safely ignore recurrent scattering processes⁴² in which a photon is bouncing back and forth between the atoms⁴³.

3. Overall solution

When solving (21) with the aid of the Laplace transform, we introduce two distinct Laplace-transform variables z_1 and z_2 to describe, respectively, the evolution after the first pulse (over τ) and after the second pulse (over t_{fl}). In our stroboscopic model of the dynamics, we obtain the overall solution for a two-atom operator by combining expressions (20) and (19), for the first and second laser pulse, with Laplace transforms of the evolutions during the interpulse delay and detection period (22). The resulting two-dimensional Laplace image reads, at order m in the dipolar coupling,

$$\tilde{Q}^{[m]}(z_1, z_2, \varphi_1, \varphi_2) = \sum_{n=0}^m \mathcal{G}_\gamma(z_2) \left[\mathcal{L}_{\text{int}} \mathcal{G}_\gamma(z_2) \right]^{m-n} R_2^L \mathcal{G}_\gamma(z_1) \left[\mathcal{L}_{\text{int}} \mathcal{G}_\gamma(z_1) \right]^n R_{1,g}^L Q(0), \quad (24)$$

where $R_2^L = \otimes_{\alpha=1}^2 R_\alpha^L$, $R_{1,g}^L = \otimes_{\alpha=1}^2 R_{1,g}^\alpha$, and $m = 0, 1, 2$. Note that the phase tags φ_1, φ_2 in the argument of the LHS of Eq. (24) are absorbed in $R_{1,g}^L$ and R_2^L via (20) and (19), respectively. Evaluation of the relevant atomic dipole correlators entering (6) according to Eq. (24), followed by the configuration average $\langle \dots \rangle_{\text{conf}}$, yields the two-dimensional Laplace image $\tilde{I}_{\mathbf{k}}(z_1, z_2, \varphi_1, \varphi_2)$ of the transient fluorescence intensity.

E. Configuration average

The configuration average is crucial to capture essential properties of a thermal atomic cloud, and to obtain reasonable

agreement with experiment. In a thermal gas, atoms have random, time-dependent positions. Thus, the averaging accounts for the intrinsic randomness of the atomic positions in a disordered medium, as well as for their changes during fluorescence harvesting (section II D 1).

As a result of the configuration average $\langle \dots \rangle_{\text{conf}}$ in (6), the structure of the expression for $\tilde{I}_{\mathbf{k}}(z_1, z_2, \varphi_1, \varphi_2)$ is substantially modified. In particular, all position-dependent phases vanish, such that the function $\tilde{I}_{\mathbf{k}}(z_1, z_2, \varphi_1, \varphi_2)$ cannot retain contributions from two-atom correlators in Eq. (6), since they are multiplied by the phase factors $\exp(i\mathbf{k} \cdot \mathbf{r}_{\alpha\beta}(t))$, with $\mathbf{r}_{\alpha\beta}(t)$ being averaged over. Nor can it depend on the phases $\varphi_{j\alpha} \equiv \varphi_j$, which, by (18), are proportional to the initial coordinates $\mathbf{r}_{\alpha 0}$.

Thus, the averaged function $\tilde{I}_{\mathbf{k}}(z_1, z_2, \varphi_1, \varphi_2)$ can either depend on the difference $\varphi_{21}^{(\alpha)} = \varphi_{2\alpha} - \varphi_{1\alpha} = \omega_0\tau + w_{21}\tau_m + \Delta_\alpha\tau$ ($\alpha = 1, 2$), or does not include $\varphi_{j\alpha}$ at all; henceforth, we denote this function by $\tilde{I}_{\mathbf{k}}(z_1, z_2, \varphi_{21}^{(1)}, \varphi_{21}^{(2)})$. Since (24) includes one superoperator $R_{1,g}^L = \otimes_{\alpha=1}^2 R_{1,g}^\alpha$, with $R_{1,g}^\alpha$ given by (20), the dependence of the average intensity $\tilde{I}_{\mathbf{k}}(z_1, z_2, \varphi_{21}^{(1)}, \varphi_{21}^{(2)})$ on $\varphi_{21}^{(\alpha)}$ can only be in the form of the phase factors $\exp(il\varphi_{21}^{(\alpha)})$, with $l = -1, 0, 1$. Nor can the function $\tilde{I}_{\mathbf{k}}(z_1, z_2, \varphi_{21}^{(1)}, \varphi_{21}^{(2)})$ depend on terms linear in $\mathcal{L}_{\text{int}} \propto g(\xi) = ie^{-i\xi}/\xi$, since $\xi = k_0 r_{\alpha\beta}$. However, terms which are independent of, or quadratic in, \mathcal{L}_{int} yield single and double scattering contributions proportional to $|g(\xi)|^0 = 1$ and $|g(\bar{\xi})|^2 = 1/\bar{\xi}^2$, respectively, where $\bar{\xi} = k_0 \bar{r}$, with \bar{r} the mean interatomic distance. Note

that, although the function $|g(\xi)|^2 = |\mathbf{r}_{\alpha 0} - \mathbf{r}_{\beta 0} + (\mathbf{v}_\alpha - \mathbf{v}_\beta)t|^2$ depends on the atomic velocities, we assume that the atoms remain in the far-field of each other, such that $|g(\xi)|^2$ varies smoothly with ξ , justifying the replacement $|g(\xi)|^2 \rightarrow |g(\bar{\xi})|^2$ in the double scattering contribution. Furthermore, among terms that are quadratic in \mathcal{L}_{int} , only particular products of the matrix elements of $\tilde{\mathbf{T}}(\bar{\xi}, \hat{\mathbf{n}})$ survive the averaging over the isotropic distribution of the vector $\hat{\mathbf{n}}$ ⁴⁴.

Decomposing $\tilde{I}_{\mathbf{k}}(z_1, z_2, \varphi_{21}^{(1)}, \varphi_{21}^{(2)})$ into single and double scattering contributions (furnished with superscripts '[0]' and '[2]', respectively, from the contributions of order $[m]$ in (24), to each correlator entering (6)), we obtain

$$\tilde{I}_{\mathbf{k}}(z_1, z_2, \varphi_{21}^{(1)}, \varphi_{21}^{(2)}) = \tilde{I}_{\mathbf{k}}^{[0]}(z_1, z_2, \varphi_{21}^{(1)}) + \tilde{I}_{\mathbf{k}}^{[2]}(z_1, z_2, \varphi_{21}^{(1)}, \varphi_{21}^{(2)}), \quad (25)$$

with

$$\tilde{I}_{\mathbf{k}}^{[0]}(z_1, z_2, \varphi_{21}^{(1)}) = \sum_{l=-1}^1 \tilde{I}_{l;\mathbf{k}}^{[0]}(z_1, z_2) e^{i\varphi_{21}^{(1)}l}, \quad \tilde{I}_{\mathbf{k}}^{[2]}(z_1, z_2, \varphi_{21}^{(1)}, \varphi_{21}^{(2)}) = \sum_{l_1=-1}^1 \sum_{l_2=-1}^1 \tilde{I}_{l_1, l_2; \mathbf{k}}^{[2]}(z_1, z_2) e^{i\varphi_{21}^{(1)}l_1 + i\varphi_{21}^{(2)}l_2}, \quad (26)$$

where the expansion “coefficients” $\tilde{I}_{l;\mathbf{k}}^{[0]}(z_1, z_2)$ and $\tilde{I}_{l_1, l_2; \mathbf{k}}^{[2]}(z_1, z_2)$, defined up to a common prefactor of 2 which accounts for permutations of atoms, are functions that are independent of the phases $\varphi_{21}^{(\alpha)}$. The phase factors in (26) (and those alone) depend on the Doppler shifts Δ_α as

$$e^{i\varphi_{21}^{(\alpha)}l} = e^{i(\omega_0\tau + w_{21}\tau_m + \Delta_\alpha\tau)l}. \quad (27)$$

It remains to integrate Eq. (26) over the one-dimensional Maxwell-Boltzmann distributions,

$$p(\Delta_\alpha) = \frac{1}{\bar{\Delta}\sqrt{2\pi}} \exp\left(-\frac{\Delta_\alpha^2}{2\bar{\Delta}^2}\right), \quad (28)$$

where $\bar{\Delta} = (k_L^2 k_B T/M)^{1/2}$ is the root-mean-square (r.m.s.) Doppler shift, with T the temperature and M the atomic mass. To that end, we evaluate the MQC spectra for fixed, random Doppler shifts and, then, average the spectra over the shifts’ distribution (28). This allows us to show, in the next subsection, how the homogeneous profiles of MQC spectra for immobile atoms transform into the inhomogeneously broadened ones observed in thermal vapors⁴⁵.

F. Signal demodulation

The phase modulation explained in Sec. II A affects the expression $\tilde{I}_{\mathbf{k}}(z_1, z_2, \varphi_{21}^{(1)}, \varphi_{21}^{(2)})$ as given by (25), (26) through the phase factors (27). Therefore, the fluorescence signal is oscillating at harmonics of the frequency w_{21} . The demodulation procedure allows one to extract specific frequency components from the full signal. The corresponding spectra, generally referred to as multiple quantum coherences (MQC), are given

by Eqs. (2) and (3). Merging these equations into one formula, replacing the phase tags ϕ_1 and ϕ_2 with the phase differences $\varphi_{21}^{(\alpha)}$, and averaging over the Doppler shifts’ distribution (28), we obtain

$$S_{\mathbf{k}}(\omega; \kappa) = \lim_{\mathcal{F} \rightarrow 0} \frac{\mathcal{F}}{\sqrt{2\pi}} \int_0^\infty d\tau_m e^{-(\mathcal{F} + i\kappa w_{21})\tau_m} \int_0^\infty d\tau e^{-i\omega\tau} \times \int_0^\infty dt_{\text{fl}} \int_{-\infty}^\infty d\Delta_1 p(\Delta_1) \int_{-\infty}^\infty d\Delta_2 p(\Delta_2) \times I_{\mathbf{k}}(\tau, t_{\text{fl}}, \varphi_{21}^{(1)}(\Delta_1), \varphi_{21}^{(2)}(\Delta_2)), \quad (29)$$

where $\kappa = 1, 2$ in this work, and $I_{\mathbf{k}}(\tau, t_{\text{fl}}, \varphi_{21}^{(1)}, \varphi_{21}^{(2)})$ is the two-dimensional inverse Laplace transform of $\tilde{I}_{\mathbf{k}}(z_1, z_2, \varphi_{21}^{(1)}, \varphi_{21}^{(2)})$; thus, it has exactly the same dependence on the phases $\varphi_{21}^{(1)}$, $\varphi_{21}^{(2)}$. By virtue of (27), this filtering procedure selects terms of the intensity modulated as $e^{i(\omega_0 + \Delta_1)\tau}$ for $\kappa = 1$, and those modulated as $e^{i(2\omega_0 + \Delta_1 + \Delta_2)\tau}$, for $\kappa = 2$.

We first assess (29) by changing the integration order, to take the integrals over Δ_1 and Δ_2 at the very end. This allows us to express $S_{\mathbf{k}}(\omega; \kappa)$ as the average over MQC spectra of atoms with fixed velocities. The latter spectra follow directly from the Laplace image $\tilde{I}_{\mathbf{k}}(z_1, z_2, \varphi_{21}^{(1)}, \varphi_{21}^{(2)})$, upon the replacements $z_1 \rightarrow i(\omega - \omega_0 - \Delta_1)$ and $z_1 \rightarrow i(\omega - 2\omega_0 - \Delta_1 - \Delta_2)$, for $\kappa = 1$ and $\kappa = 2$, respectively, and $z_2 \rightarrow 0$ because of the infinite upper integration limit in (2).

The selection of terms in (29) with a specific modulated phase due to (26), (27) implies that only certain sum indices in (26) can contribute to κ QC signals: The condition $l = \kappa$ and $l_1 + l_2 = \kappa$ must be fulfilled for the single and double scattering contributions, respectively. Therefore, using Eqs. (25)–(29), we obtain that the 1QC and 2QC signals are given by

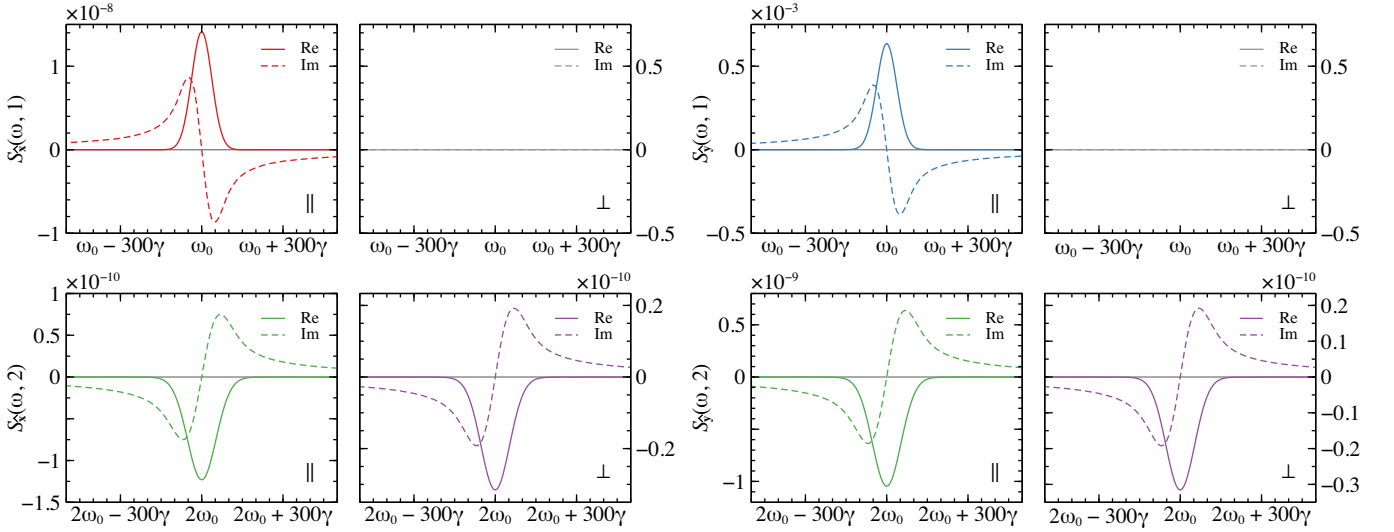


Figure 2. Real (Re, solid lines) and imaginary (Im, dashed lines) parts of the MQC spectra $S_{\hat{k}}(\omega; \kappa)$ [in units of the spectral density integrated over the fluorescence detection time, f^2/γ^2 ; see (6) and (29)] of $N = 2$ atoms, for detection direction $\hat{k} = \hat{x}$ (left), $\hat{k} = \hat{y}$ (right), and for quantum coherences of order $\kappa = 1$ (top), $\kappa = 2$ (bottom). Symbols \parallel and \perp indicate parallel ($\hat{x}\hat{x}$) and perpendicular ($\hat{x}\hat{y}$) pump-probe polarizations, respectively. All plots were obtained for temperature $T = 320$ K, average interatomic distance $\bar{r} \approx 10 \mu\text{m}$ (which corresponds to the particle density 10^8 cm^{-3}), laser pulse areas $\vartheta = 0.14\pi$ and durations $\sigma = 21 \text{ fs}$ (tuned to resonance with the D2-line of ^{87}Rb atoms³⁷), atomic mass $M = 1.443 \times 10^{-25} \text{ kg}$, transition wavelength $\lambda_0 = 790 \text{ nm}$, and the spontaneous decay rate $\gamma \approx 2\pi \times 6.067 \text{ MHz}$, faithfully matching the experimental conditions¹⁶. This choice of parameters results in a mean scaled interatomic distance $\bar{\xi} = k_0\bar{r} \approx 80$, with k_0 the atomic transition's wave number, and a r.m.s. Doppler shift $\bar{\Delta} = 2\pi \times 0.221 \text{ GHz}$.

the following convolutions of Lorentzian (for a given velocity/Doppler shift) and Gaussian distributions (28),

III. RESULTS AND DISCUSSION

A. Inhomogeneously broadened 1QC and 2QC spectra

$$S_{\hat{k}}(\omega; 1) = \int_{-\infty}^{\infty} d\Delta_1 p(\Delta_1) \left[\tilde{I}_{1,\hat{k}}^{[0]} \left(i(\omega - \omega_0 - \Delta_1), 0 \right) + \tilde{I}_{1,0,\hat{k}}^{[2]} \left(i(\omega - \omega_0 - \Delta_1), 0 \right) \right], \quad (30)$$

$$S_{\hat{k}}(\omega; 2) = \int_{-\infty}^{\infty} d\Delta_1 p(\Delta_1) \int_{-\infty}^{\infty} d\Delta_2 p(\Delta_2) \times \tilde{I}_{1,1,\hat{k}}^{[2]} \left(i(\omega - 2\omega_0 - \Delta_1 - \Delta_2), 0 \right). \quad (31)$$

The above expressions yield complex κ QC spectra with resonances at $\omega = \kappa\omega_0$; the real, absorptive parts of the spectral line shapes are also known as Voigt profiles⁵. If we take the limit $T \rightarrow 0$ in (28), the distribution $p(x) \rightarrow \delta(x)$, and the expressions (30) and (31) for κ QC spectra reduce to the complex Lorentzians reported elsewhere²⁰. Equation (30) indicates that 1QC spectra can emerge from either independent or interacting atoms, whereas equation (31) only contains double scattering contributions, such that 2QC spectra do require interactions via photon exchange.

Next, based on the above results, we examine 1QC and 2QC spectra for different pump-probe polarizations, observation directions, and pulse areas.

Using symbolic computation software, we analytically assess the single and double quantum coherence spectra $S_{\hat{k}}(\omega; 1)$ and $S_{\hat{k}}(\omega; 2)$ of $N = 2$ atoms, as given by Eqs. (30) and (31), for arbitrary pulse areas ϑ , for detection directions $\hat{k} = \hat{x}, \hat{y}$, and for parallel ($\hat{x}\hat{x}$) and perpendicular ($\hat{x}\hat{y}$) pump-probe polarization channels (in brief, \parallel and \perp channels). First, however, we consider parameter values close to the experimental ones¹⁶, which, in particular, correspond to a fixed pulse area $\vartheta = 0.14\pi$. The spectra that result in this case are shown in Fig. 2.

Whenever they do not vanish identically, the complex 1QC and 2QC spectra feature, respectively, absorptive and dispersive resonances of the real and imaginary parts. We recall that, by (30), 1QC signals can result from single scattering (one atom interacts with two laser fields, Fig. 3 (a)) as well as from double scattering (one atom driven by two fields scattered by the other atom, Fig. 3 (b)). In the case of $S_{\hat{y},\parallel}(\omega; 1)$, single scattering dominates the signal, since both incoming pulses are polarized along the \hat{x} -axis, while double scattering only yields a small correction. In contrast, non-interacting atoms driven by \hat{x} -polarized fields cannot emit in the \hat{x} direction. The signal can then only emerge from the \hat{y} and \hat{z} components of the transition dipoles, which can be excited via double scattering, wherefrom the $S_{\hat{x},\parallel}(\omega; 1)$ signal stems. In the weak-field limit, the 1QC spectrum $S_{\hat{y},\parallel}(\omega; 1)$ scales as ϑ^2 , whereas $S_{\hat{x},\parallel}(\omega; 1)$ scales as $\vartheta^2/\bar{\xi}^2$, so that both are proportional to the linear

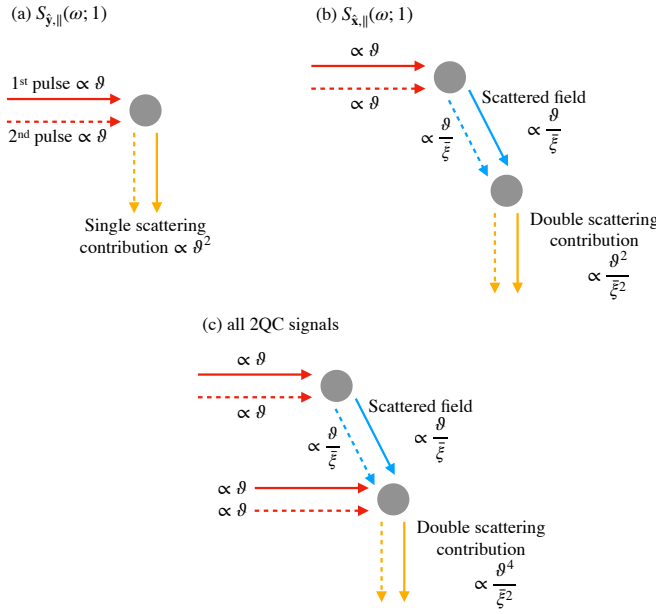


Figure 3. Scaling of 1QC signals (a) $S_{\hat{y},\parallel}(\omega; 1)$, (b) $S_{\hat{x},\parallel}(\omega; 1)$, as well as all (c) 2QC signals, with the pulse area ϑ and the mean scaled interatomic distance ξ , in the weak, $\vartheta \ll 1$, and far-field, $\xi \gg 1$, limit. Signal (a) originates from single scattering, signals (b,c) from double scattering. Horizontal red lines indicate the incoming laser pulses, vertical yellow lines the emitted fluorescence, oblique blue lines the scattered fields via dipole-dipole interactions. Solid and dashed lines distinguish a single field amplitude from its complex conjugate.

susceptibility¹². By (31), the 2QC spectra always originate from double scattering, where, in this context, an atom is subject to two laser fields and two fields scattered by the other atom (Fig. 3 (c)). In the weak-field limit, the 2QC spectra scale with the pulse area as ϑ^4/ξ^2 , and are therefore proportional to the third-order non-linear susceptibility^{5,46}. Since the signs of the first- and third-order susceptibilities are opposite⁴⁶, so are the signs of the 1QC and 2QC spectra (see Fig. 2).

In order to compare the magnitudes of the κ QC peaks let us introduce the shorthand

$$A_{\hat{k},\parallel/\perp}(\kappa) = \text{Re}\{S_{\hat{k},\parallel/\perp}(\kappa\omega_0; \kappa)\} \quad (32)$$

for the amplitude of the real part of these spectra. Note that the dependence on the pulse area is not spelled out explicitly for brevity.

For a single fine transition (D2-line) of rubidium atoms, the positions, lineshapes, and signs of all resonances in Fig. 2, as well as the absence of the 1QC signals in the \perp channel are in qualitative agreement with the experimental observations^{16,45}. Furthermore, the ratio of the peak values of 2QC and 1QC signals, $A_{\hat{x},\parallel}(2)/A_{\hat{x},\parallel}(1) \sim 10^{-2}$, approximately equals the experimental value¹⁶. Finally, the calculated inhomogeneously broadened spectral lines have absorptive parts with dominantly Gaussian line shapes, whose full widths at half maximum are about 100γ , or ≈ 1.39 GHz. This also agrees, in order of magnitude, with the experimentally observed line widths⁴⁵.

Let us briefly recap which are the crucial ingredients to capture the essential physics and to obtain reasonable qualitative

and quantitative agreement with experiment:

- First of all, to obtain the κ QC spectra for different channels and observation directions, one needs to incorporate the vector nature of atomic dipole transitions, of which the here considered atoms equipped with a $J_g = 0 \leftrightarrow J_e = 1$ transition represent the simplest example.
- Second, performing the configuration average is extremely important to account for both, the randomness of atomic positions, and their drift in a thermal gas. Without this procedure, neither the line shapes nor their magnitudes have any resemblance with the observed ones. For instance, for individual random realizations, both $S_{\hat{x}}(\omega; 1)$ and $S_{\hat{y}}(\omega; 1)$ would yield non-zero contributions in the \perp channel, and it is only the configuration average which completely suppresses this specific signal.
- Third, given the diluteness of the atomic sample, the dominant contribution to the dipole-dipole interaction is due to its far-field part describing real photon exchange. By considering only the near-field (electrostatic) term instead, one substantially underestimates the magnitude of MQC signals. More importantly, unlike the electrostatic interaction which brings about collective levels shifts, the far-field dipole-dipole interactions lead to both, collective shifts *and* collective decay processes. Let us note in passing that collective decay plays a crucial role even for very close emitters, where it can trigger coherent excitation flow under incoherent driving⁴⁷.

B. Dependence of the peak amplitudes on the pulse area

Let us now exploit the potential of our non-perturbative approach and examine the behavior of the real parts of the 1QC and 2QC spectra for $N = 2$ atoms under changes of the pulse area ϑ .

In table I, we provide the expressions for the peak amplitudes $A_{\hat{k},\parallel/\perp}(\kappa)$ as defined in (32), to leading order in ξ^{-2} . These expressions are oscillatory functions of ϑ with periods varying from π (for $A_{\hat{y},\parallel}(1)$, $A_{\hat{x},\parallel}(2)$, and $A_{\hat{y},\parallel}(2)$), over 2π (for $A_{\hat{x},\perp}(2)$ and $A_{\hat{x},\perp}(2)$), to 4π (for $A_{\hat{x},\parallel}(1)$). Due to their different scaling with the inverse square of the scaled interatomic distance, ξ^{-2} , and/or different numerical prefactors, these functions vary significantly in magnitude (see also the variable scales of the y-axis in Fig. 2). Therefore, to compare their behavior solely as functions of ϑ , Fig. 4 (left) normalizes the functions to unit amplitude, retaining the overall sign.

We notice that all functions vanish at $\vartheta = n\pi$ ($n = 0, 1, 2, \dots$). The occurrence of the zeroes at integer multiples of π can be understood as an immediate consequence of the Rabi dynamics of coherently driven two-level atoms⁴⁸, together with the fact that the atoms are interacting with two identical time-delayed pulses. Since typically these delays $\tau \sim 10$ ps are short (see Sec. II D 1), spontaneous emission events between the pulses can be ignored. Thus, the first

κ	$\hat{\mathbf{k}}$	channel	$A_{\hat{\mathbf{k}}, \parallel/\perp}(\kappa) / (f^2 / \sqrt{2\pi}\gamma^2)$
1	$\hat{\mathbf{x}}$	\parallel	$\frac{1}{80\tilde{\xi}^2} \sin^2 \vartheta \left[\frac{3\gamma^2}{\Delta^2} \cos^3 \frac{\vartheta}{2} \right.$ $- 3V\left(\frac{\gamma}{2\Delta}\right) \cos \frac{\vartheta}{2} \left(\frac{\gamma^2}{\Delta^2} + (1 - 4 \cos \frac{\vartheta}{2} - \cos \vartheta) \right)$ $\left. + V\left(\frac{3\gamma}{2\Delta}\right) \sin^2 \frac{\vartheta}{2} \left(\frac{3\gamma^2}{\Delta^2} \cos \frac{\vartheta}{2} + (2 \cos \frac{\vartheta}{2} - 4 \cos \vartheta) \right) \right]$
	$\hat{\mathbf{y}}$	\parallel	$V(\gamma/\sqrt{2\Delta}) \sin^2 \vartheta + \mathcal{O}(\tilde{\xi}^{-2})$
	$\hat{\mathbf{x}}, \hat{\mathbf{y}}$	\perp	0
2	$\hat{\mathbf{x}}$	\parallel	$-\frac{3}{320\tilde{\xi}^2} V(\gamma/\sqrt{2\Delta}) \sin^4 \vartheta$
2	$\hat{\mathbf{y}}$	\parallel	$-\frac{51}{640\tilde{\xi}^2} V(\gamma/\sqrt{2\Delta}) \sin^4 \vartheta$
2	$\hat{\mathbf{x}}, \hat{\mathbf{y}}$	\perp	$-\frac{3}{320\tilde{\xi}^2} V(\gamma/\sqrt{2\Delta}) \sin^2 \frac{\vartheta}{2} \sin^2 \vartheta$

Table I. Peak amplitudes $A_{\hat{\mathbf{k}}, \parallel/\perp}(\kappa) = \text{Re}\{S_{\hat{\mathbf{k}}, \parallel/\perp}(\kappa\omega_0; \kappa)\}$ of the single (30) and double quantum coherence spectra (31) of $N = 2$ fluorescing atoms, with $V(x) = \sqrt{\pi/2}x \exp(x^2/2) \text{erfc}(x/\sqrt{2})$, the r.m.s. Doppler shift $\bar{\Delta} = k_L \sqrt{k_B T/M}$ defined through (28) and the constant f given below (5). For each signal we give here the leading order, which is always $\mathcal{O}(\tilde{\xi}^{-2})$ except for $A_{\hat{\mathbf{y}}, \parallel}(1)$, where the single-scattering contribution dominates as $\mathcal{O}(0)$, see Fig. 3 (a).

π -pulse⁴⁸ coherently transfers the atoms from the ground to the excited state, while the second π -pulse, conversely, coherently brings the atoms back to their ground states. Hence, the atoms cannot fluoresce, regardless of MQC order κ , polarization channel, or observation direction.

According to the same logic, the largest peak magnitudes can be expected at odd integer multiples of the “optimal” pulse area, $\vartheta_{\text{opt}} = \pi/2$. After two such pulses, the atomic population of an isolated atom is coherently transferred from the ground to the excited state, feeding a fluorescence signal which attains a maximum. And indeed, we observe maximal magnitudes for the functions $A_{\hat{\mathbf{y}}, \parallel}(1)$, $A_{\hat{\mathbf{x}}, \parallel}(2)$ and $A_{\hat{\mathbf{y}}, \parallel}(2)$ at $\vartheta = (2n+1)\vartheta_{\text{opt}}$ ($n = 0, 1, 2, \dots$), see Fig. 4 (left). However, the functions $A_{\hat{\mathbf{x}}, \parallel}(1)$ and $A_{\hat{\mathbf{x}}, \perp}(2) = A_{\hat{\mathbf{y}}, \perp}(2)$ reach their maximal magnitudes for the first time at values of $\vartheta \approx 0.4\pi$ and $\approx 0.6\pi$, respectively, that are slightly shifted with respect to the “optimal” pulse area 0.5π . We attribute this to peculiar physical mechanisms for the generation of 1QC or 2QC signals, which require excited state degeneracy and collective decay processes⁴⁴.

In order to further quantify the distinctions between the peak amplitudes, in Fig. 4 (right) we have plotted the coefficients A_n obtained by expansion of the oscillatory functions from Fig. 4 (left) in a trigonometric series

$$A(\vartheta) = \sum_n A_n \cos \frac{n\vartheta}{2}. \quad (33)$$

Despite quite similar periodic behavior of the peak amplitudes Fig. 4 (left), their expansions (33) elucidate the differences between distinct signals via the coefficients A_n . In other words, these coefficients can be conceived as specific “fingerprints” reflecting the order κ , the polarizations of the laser pulses, as well as the observation direction. Thus, the nonlinear laser-

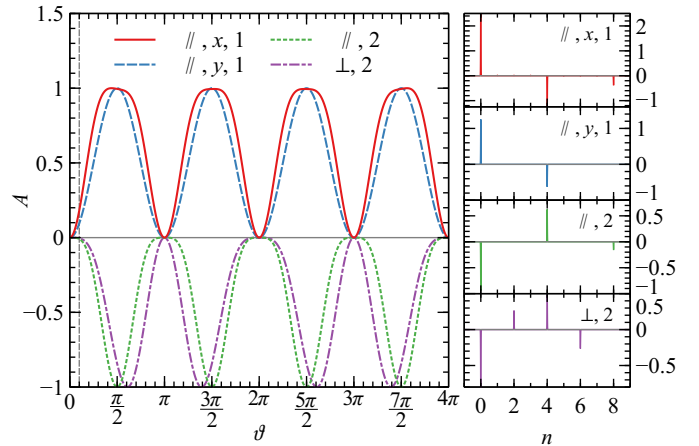


Figure 4. (Left) Peak amplitudes $A_{\hat{\mathbf{k}}, \parallel/\perp}(\kappa) = \text{Re}\{S_{\hat{\mathbf{k}}, \parallel/\perp}(\kappa\omega_0; \kappa)\}$ of the single and double quantum coherence spectra of $N = 2$ fluorescing atoms (same color code as Fig. 2), obtained from table I by normalizing their amplitude to ± 1 (hence, the 2QC signals’ amplitudes $A_{\hat{\mathbf{x}}, \parallel}(2) \propto A_{\hat{\mathbf{y}}, \parallel}(2)$ and $A_{\hat{\mathbf{x}}, \perp}(2) = A_{\hat{\mathbf{y}}, \perp}(2)$ are represented by one green dotted and one purple dash-dotted line, respectively), as functions of the pulse area ϑ , for \parallel and \perp pump-probe polarizations and detection directions $\hat{\mathbf{k}} = \hat{\mathbf{x}}, \hat{\mathbf{y}}$ (see legends). The vertical dashed line at $\vartheta = 0.14\pi$ corresponds to the pulse area in Fig. 2. The values of the other parameters are the same as in Fig. 2. (Right) Amplitudes A_n of the trigonometric expansion (33) of $A(\vartheta)$ as displayed in the left panel (identified by the color code).

atom interaction processes induced by strong driving fields modify the MQC signals, and this modification is in itself a diagnostic tool of dipolar interactions in dilute thermal gases.

IV. CONCLUSIONS

We expanded our non-perturbative open-system theory of multiple quantum coherence^{20,40} to account for thermal atomic motion, and to address the dependence of MQC signals on the driving strength as quantified by the incoming pulses’ areas. While the former leads to improved qualitative agreement between our numerical results for $N = 2$ atoms (as the minimal model to incorporate all physically relevant processes which contribute to the detected fluorescence) and experiment¹⁴, the latter defines a new diagnostic tool to discriminate different excitation channels, beyond the perturbative regime.

ACKNOWLEDGMENTS

E. G. C. acknowledges the support of the G. H. Endress Foundation. V. S. and A. B. thank the Strategiefonds der Albert-Ludwigs-Universität Freiburg for partial funding.

REFERENCES

¹M. J. Stephen, “First-order dispersion forces,” *J. Chem. Phys.* **40**, 669 (1966).

²D. A. Hutchison and H. F. Hameka, "Interaction effects on lifetimes of atomic excitations," *Chem. Phys.* **41**, 2006 (1964).

³P. W. Milonni, *The Quantum Vacuum: An Introduction to Quantum Electrodynamics* (Academic Press, San Diego, 1994).

⁴R. Friedberg, S. Hartmann, and J. Manassah, "Frequency shifts in emission and absorption by resonant systems of two-level atoms," *Phys. Rep.* **7**, 101 (1973).

⁵S. Mukamel, *Principles of Nonlinear Optical Spectroscopy* (Oxford University Press, New York, 1995).

⁶X. Dai, M. Richter, H. Li, A. D. Bristow, C. Falvo, S. Mukamel, and S. T. Cundiff, "Two-dimensional double-quantum spectra reveal collective resonances in an atomic vapor," *Phys. Rev. Lett.* **108**, 193201 (2012).

⁷S. T. Cundiff and S. Mukamel, "Optical multidimensional coherent spectroscopy," *Phys. Today* **66**, 44 (2013).

⁸F. Gao, S. T. Cundiff, and H. Li, "Probing dipole-dipole interaction in a rubidium gas via double-quantum 2D spectroscopy," *Opt. Lett.* **41**, 2954 (2016).

⁹D. M. Jonas, "Two-dimensional femtosecond spectroscopy," *Annu. Rev. Phys. Chem.* **54**, 425 (2003).

¹⁰L. Bruder, U. Bangert, M. Binz, D. Uhl, and F. Stienkemeier, "Coherent multidimensional spectroscopy in the gas phase," *J. Phys. B: At. Mol. Opt. Phys.* **52**, 183501 (2019).

¹¹S. Mueller, J. Lüttig, P. Malý, L. Ji, J. Han, M. Moos, T. B. Marder, U. H. F. Bunz, A. Dreuw, C. Lambert, and T. Brixner, "Rapid multiple-quantum three-dimensional fluorescence spectroscopy disentangles quantum pathways," *Nat. Commun.* **10**, 4735 (2019).

¹²P. F. Tekavec, G. A. Lott, and A. H. Marcus, "Fluorescence-detected two-dimensional electronic coherence spectroscopy by acousto-optic phase modulation," *J. Chem. Phys.* **127**, 214307 (2007).

¹³L. Bruder, M. Mudrich, and F. Stienkemeier, "Phase-modulated electronic wave packet interferometry reveals high resolution spectra of free Rb atoms and Rb*He molecules," *Phys. Chem. Chem. Phys.* **17**, 23877 (2015).

¹⁴L. Bruder, M. Binz, and F. Stienkemeier, "Efficient isolation of multiphoton processes and detection of collective resonances in dilute samples," *Phys. Rev. A* **92**, 053412 (2015).

¹⁵S. Yu, M. Titze, Y. Zhu, X. Liu, and H. Li, "Observation of scalable and deterministic multi-atom Dicke states in an atomic vapor," *Opt. Lett.* **44**, 2795 (2019).

¹⁶L. Bruder, A. Eisfeld, U. Bangert, M. Binz, M. Jakob, D. Uhl, M. Schulz-Weiling, E. R. Grant, and F. Stienkemeier, "Delocalized excitons and interaction effects in extremely dilute thermal ensembles," *Phys. Chem. Chem. Phys.* **21**, 2276 (2019).

¹⁷S. Mukamel, "Communication: The origin of many-particle signals in nonlinear optical spectroscopy of non-interacting particles," *J. Chem. Phys.* **145**, 041102 (2016).

¹⁸Z.-Z. Li, L. Bruder, F. Stienkemeier, and A. Eisfeld, "Probing weak dipole-dipole interaction using phase-modulated nonlinear spectroscopy," *Phys. Rev. A* **95**, 052509 (2017).

¹⁹O. Kühn, T. Mančal, and T. Pullerits, "Interpreting fluorescence detected two-dimensional electronic spectroscopy," *J. Phys. Chem. Lett.* **11**, 838 (2020).

²⁰B. Ames, E. Carnio, V. Shatokhin, and A. Buchleitner, "Sensing multiple scattering via multiple quantum coherence signals," *Preprint arXiv:2002.09662* (2020).

²¹D. A. Blank, L. J. Kaufman, and G. R. Fleming, "Fifth-order two-dimensional Raman spectra of CS₂ are dominated by third-order cascades," *J. Chem. Phys.* **111**, 3105 (1999).

²²K. Bennett and S. Mukamel, "Cascading and local-field effects in non-linear optics revisited: A quantum-field picture based on exchange of photons," *J. Chem. Phys.* **140**, 044313 (2014).

²³P. Grégoire, A. R. Srimath Kandada, E. Vella, C. Tao, R. Leonelli, and C. Silva, "Incoherent population mixing contributions to phase-modulation two-dimensional coherent excitation spectra," *J. Chem. Phys.* **147**, 114201 (2017).

²⁴S. Mueller and T. Brixner, "Molecular coherent three-quantum two-dimensional fluorescence spectroscopy," *J. Phys. Chem. Lett.* **11**, 5139 (2020).

²⁵To avoid confusion, we use a special notation t_{fl} for the fluorescence detection time, while we retain the notation t for a general time variable.

²⁶P. F. Tekavec, T. R. Dyke, and A. H. Marcus, "Wave packet interferometry and quantum state reconstruction by acousto-optic phase modulation," *J. Chem. Phys.* **125**, 194303 (2006).

²⁷G. S. Agarwal, *Quantum Statistical Theories of Spontaneous Emission and their Relation to other Approaches* (Springer, Berlin, 1974).

²⁸R. J. Glauber, *Quantum theory of optical coherence* (Wiley-VCH, Weinheim, 2007).

²⁹M. Trippenbach, B. Gao, J. Cooper, and K. Burnett, "Slow collisions between identical atoms in a laser field: Application of the Born and Markov approximations to the system of moving atoms," *Phys. Rev. A* **45**, 6539 (1992).

³⁰R. H. Lehmburg, "Radiation from an N -atom system. I. general formalism," *Phys. Rev. A* **2**, 883 (1970).

³¹H. P. Breuer and F. Petruccione, *The Theory of Open Quantum Systems* (Oxford University Press, Oxford, 2002).

³² $\bar{r} \simeq 0.554 n^{-1/3}$,⁴⁹ which for a particle density $n \simeq 10^8 \text{ cm}^{-3}$ is about 10 μm .

³³V. Shatokhin, C. A. Müller, and A. Buchleitner, "Elastic versus inelastic coherent backscattering of laser light by cold atoms: A master-equation treatment," *Phys. Rev. A* **73**, 063813 (2006).

³⁴V. Shatokhin, C. A. Müller, and A. Buchleitner, "Coherent inelastic backscattering of intense laser light by cold atoms," *Phys. Rev. Lett.* **94**, 043603 (2005).

³⁵J. Guo and J. Cooper, "Cooling and resonance fluorescence of two atoms in a one-dimensional optical molasses," *Phys. Rev. A* **51**, 3128 (1995).

³⁶D. L. Andrews and D. S. Bradshaw, "Virtual photons, dipole fields and energy transfer: a quantum electrodynamical approach," *Eur. J. Phys.* **25**, 845 (2004).

³⁷D. A. Steck, "Rubidium 87 D Line Data," available online at <http://steck.us/alkalidata/>.

³⁸G. Labeyrie, D. Delande, R. Kaiser, and C. Miniatura, "Light transport in cold atoms and thermal decoherence," *Phys. Rev. Lett.* **97**, 013004 (2006).

³⁹The thermal coherence time $\tau_{\text{th}} = \lambda/v \approx 10 \text{ ns}$ can be obtained from the Doppler shift $k_0 v \approx 560 \text{ MHz}$ and the wavelength $\lambda = 2\pi/k_0 \approx 790 \text{ nm}$ ¹⁶.

⁴⁰B. Ames, *Dynamical detection of dipole-dipole interactions in dilute atomic gases*, Master's thesis, Albert-Ludwigs-Universität Freiburg (2019).

⁴¹T. Jonckheere, C. A. Müller, R. Kaiser, C. Miniatura, and D. Delande, "Multiple scattering of light by atoms in the weak localization regime," *Phys. Rev. Lett.* **85**, 4269 (2000).

⁴²D. V. Kupriyanov, I. M. Sokolov, and M. D. Havey, "Mesoscopic coherence in light scattering from cold, optically dense and disordered atomic systems," *Phys. Rep.* **671**, 1 (2017).

⁴³B. A. van Tiggelen and A. Lagendijk, "Resonantly induced dipole-dipole interactions in the diffusion of scalar waves," *Phys. Rev. B* **50**, 16729 (1994).

⁴⁴B. Ames, E. G. Carnio, V. Shatokhin, and A. Buchleitner, "Theory of multiple quantum coherence signals in dilute thermal gases," in preparation (2021).

⁴⁵L. Bruder, *Nonlinear phase-modulated spectroscopy of doped helium droplet beams and dilute gases*, Ph.D. thesis, Albert-Ludwigs-Universität Freiburg (2017).

⁴⁶R. W. Boyd, *Nonlinear Optics*, 2nd ed. (Academic Press, San Diego, 2003).

⁴⁷V. N. Shatokhin, M. Walschaers, F. Schlawin, and A. Buchleitner, "Coherence turned on by incoherent light," *New J. Phys.* **20**, 113040 (2018).

⁴⁸L. Allen and J. Eberly, *Optical Resonance and Two-Level Atoms* (Dover Publications, Inc., New York, 1987).

⁴⁹J. A. Leegwater and S. Mukamel, "Self-broadening and exciton line shifts in gases: Beyond the local-field approximation," *Phys. Rev. A* **49**, 146 (1994).